Theory of band comparison in even-even nuclei

B. Buck,[1] A. C. Merchant,[1] and S. M. Perez[2]
[1]*Department of Physics, University of Oxford, Theoretical Physics, 1 Keble Road, Oxford OX1 3NP, United Kingdom*
[2]*Department of Physics, University of Cape Town, Private Bag, Rondebosch 7700, South Africa*
(Received 23 November 2002; published 25 August 2003)

We previously found that a cluster model reproduces satisfactorily the properties of normal deformed (ND) ground state and superdeformed (SD) excited bands in a wide range of even-even nuclei. We show here that the fractional change of the transition energies in two bands described by similar core-cluster configurations is closely related to the fractional change in the corresponding reduced masses. We compare our predictions to data on ground state ND bands for a series of light rare-earth and actinide isotopes, and on SD bands in the $A\sim150$ and 190 regions. The model strongly suggests the existence of similar excited SD bands in ^{212}Pb and ^{212}Po, in addition to the observed α-cluster-like ND ground state bands of these nuclei.

DOI: 10.1103/PhysRevC.68.024313 PACS number(s): 21.60.Gx, 23.20.Js, 27.50.+e

I. INTRODUCTION

Generally, the structures of nearby even-even nuclei bear marked similarities to one another. In particular, ground state bands with very similar energy spacings and electromagnetic properties are often seen across a sequence of isotopes. In extreme circumstances, the energy differences between excited bands in different nuclei may be so similar that they are barely resolvable with present experimental techniques. In this paper, we are principally concerned with categorizing the degree of similarity of two bands. We propose to do this by comparing the ratios of the energy difference to the mean energy for states of specified angular momenta in the two bands. The difference in the ratios provides a numerical measure of the degree of similarity of the energy levels of the two bands. Equal ratios obviously imply that the bands are identical [1–3].

We have previously shown that a cluster model description is widely applicable to nuclei containing normally deformed (ND) and superdeformed (SD) quasirotational bands [4]. We shall show here that the reduced masses implied by such a cluster-core picture can be simply related to the numerical measure of the degree of similarity of the two bands introduced above. We begin with a short discussion of how to choose appropriate core and cluster for an arbitrary nucleus, and then give a brief overview of the model. We confine our attention to even-even nuclei since their treatment is more straightforward, but there are no problems, in principle, in extending it to the odd-A case.

We illustrate the correlation of fractional energy changes between band members and cluster-core reduced mass with typical examples drawn from the ground state bands of light rare-earth and actinide nuclei. We also examine very similar bands of superdeformed states in the mass 150 and 190 regions, where the fractional energy changes of 1–2 % are comparable to those expected for a uniform sphere having moment of inertia $2MR^2/5$. Finally, model considerations indicate that an excellent illustration of closely similar bands should be present in ^{212}Pb and ^{212}Po, and we present predictions for these two nuclei.

II. CHOICE OF CLUSTER AND CORE

In order to describe a given band in a nucleus of charge Z_T and mass A_T with a cluster model, we must first specify the core (Z_1,A_1) and the cluster (Z_2,A_2) appropriate to the band. We have proposed [5,6] that likely binary clusterizations of a given parent nucleus can be identified by determining the local maxima of the function $D(Z_1,A_1,Z_2,A_2)$ defined by

$$D(Z_1,A_1,Z_2,A_2)=[B_E(Z_1,A_1)-B_L(Z_1,A_1)]+[B_E(Z_2,A_2)-B_L(Z_2,A_2)], \quad (1)$$

where B_E is an experimentally determined binding energy and B_L the corresponding liquid drop value for each of the fragments of (charge, mass) (Z_i,A_i) with $i=1,2$ into which the parent of (charge, mass) (Z_T,A_T) may be divided. Likely clusterizations then correspond to the largest deviations of the summed binding energies of the two fragments from liquid drop values. A convenient form for B_L is [7]

$$B_L=a_vA-a_sA^{2/3}-a_c\frac{Z^2}{A^{1/3}}-a_a\frac{(A-2Z)^2}{A}+\delta, \quad (2)$$

where

$$a_v=15.56\ \text{MeV}, \quad a_s=17.23\ \text{MeV},$$
$$a_c=0.697\ \text{MeV}, \quad a_a=23.285\ \text{MeV}. \quad (3)$$

The pairing term δ in Eq. (2) is taken as $12/\sqrt{A}$ for even-even nuclei. In addition, electric dipole transitions between low-lying bands are known to be very weak, suggesting that attention should be restricted to fragments obeying the condition

$$\frac{Z_1}{A_1}=\frac{Z_2}{A_2}=\frac{Z_T}{A_T}, \quad (4)$$

so that the implied dipole transition rates, which involve the operator $(Z_1/A_1-Z_2/A_2)$, vanish identically.

The restriction, Eq. (4), cannot usually be achieved for an arbitrary parent nucleus using integer charge and mass numbers for the cluster and core components. Reference [6] describes how we nevertheless obtain a continuous function $\langle D(Z_1,A_1,Z_2,A_2)\rangle$ for arbitrary values of the cluster charge $\langle Z_2\rangle$ by writing

$$\langle D(Z_1,A_1,Z_2,A_2)\rangle = \sum_{Z_2,N_2} p(Z_2)p(N_2)D(Z_1,A_1,Z_2,A_2). \tag{5}$$

This is a weighted average of $D(Z_1,A_1,Z_2,A_2)$ for the four even-even nuclei (Z_2-2,N_2-2), (Z_2,N_2-2), (Z_2-2,N_2), and (Z_2,N_2), which bracket $\langle Z_2\rangle$ and $\langle N_2\rangle = \langle Z_2\rangle(N_T/Z_T)$, such that

$$Z_2 \geqslant \langle Z_2\rangle \geqslant Z_2-2 \quad \text{and} \quad N_2 \geqslant \langle N_2\rangle \geqslant N_2-2. \tag{6}$$

The corresponding probabilities (weights) are

$$p(Z_2) = (1/2)[\langle Z_2\rangle - (Z_2-2)],$$

$$p(Z_2-2) = (1/2)[Z_2 - \langle Z_2\rangle],$$

$$p(N_2) = (1/2)[\langle N_2\rangle - (N_2-2)],$$

$$p(N_2-2) = (1/2)[N_2 - \langle N_2\rangle]. \tag{7}$$

III. CLUSTER MODEL

Having determined the nature of the core and the cluster from a D plot, or by other means, we next require their mutual interaction. We have proposed [8] a universal form for the nuclear part $V_N(r)$ of this interaction, which for $A_1,A_2 \gg 1$ is given by

$$V_N(r) = -V_0\left(\frac{A_1A_2}{A_T}\right)\frac{f(r,R,x,a)}{f(0,R,x,a)}, \tag{8}$$

with

$$f(r,R,x,a) = \left[\frac{x}{\{1+\exp[(r-R)/a]\}} + \frac{1-x}{\{1+\exp[(r-R)/3a]\}^3}\right], \tag{9}$$

having specific parameter values

$$V_0 = 54.0 \text{ MeV}, \quad x = 0.33, \quad a = 0.73 \text{ fm}. \tag{10}$$

The core-cluster interaction also includes a Coulomb term $V_C(r)$ given by

$$V_C(r) = Z_1Z_2e^2h(r,R), \tag{11}$$

where $h(r,R)$ is the functional form appropriate to the Coulomb interaction between a uniformly charged sphere of charge Z_1 and radius R and a point charge Z_2. A value of the radius parameter R completes the specification of the core-cluster interaction. For a given band, this value can be determined by fitting a single state of the band, once the global quantum number $G=2n+l$ of the band has been selected [4] (n is the radial and l the orbital angular momentum quantum number of a member of the band).

Our comparison of corresponding bands in even-even nuclei requires only the general form of the core-cluster interaction given by Eqs. (8) and (11). These may be rewritten as

$$V_N(r) = -V_0\left(\frac{A_1A_2}{A_T}\right)\frac{f(r,R,x,a)}{f(0,R,x,a)} = \mu F_N(r) \tag{12}$$

and

$$V_C(r) = Z_1Z_2e^2h(r,R) = \frac{A_1A_2}{A_T}\frac{Z_T^2}{A_T}e^2h(r,R) = \mu F_C(r), \tag{13}$$

where $\mu=(A_1A_2)/A_T$ is the reduced mass of the core-cluster system in atomic mass units, and we have used the dipole constraint of Eq. (4) in deriving Eq. (13).

IV. THEORETICAL BAND COMPARISON METHOD

Consider two bands B and $\hat{B}$ in the same nucleus, which are assumed to differ slightly in their value of the reduced masses μ and $\hat{\mu}$, respectively. For angular momentum l, let the two solutions to the radial Schrödinger equation be χ_l, $\hat{\chi}_l$ with corresponding energies E_l and $\hat{E}_l$. Then, multiplying each radial Schrödinger equation by the wave function of the other results in the equations

$$\chi_l\frac{d^2\hat{\chi}_l}{dr^2} - \left\{\frac{2\hat{\mu}^2}{\hbar^2}[F_N(r)+F_C(r)] + \frac{l(l+1)}{r^2}\right\}\hat{\chi}_l\chi_l = -\frac{2\hat{\mu}}{\hbar^2}\hat{E}_l\hat{\chi}_l\chi_l \tag{14}$$

and

$$\hat{\chi}_l\frac{d^2\chi_l}{dr^2} - \left\{\frac{2\mu^2}{\hbar^2}[F_N(r)+F_C(r)] + \frac{l(l+1)}{r^2}\right\}\hat{\chi}_l\chi_l = -\frac{2\mu}{\hbar^2}E_l\hat{\chi}_l\chi_l. \tag{15}$$

Subtracting these two equations, dividing out the common factor $2/\hbar^2$, and integrating with respect to r from 0 to ∞ leads to

$$(\hat{\mu}^2-\mu^2)\int_0^\infty [F_N(r)+F_C(r)]\hat{\chi}_l\chi_l\,dr = (\hat{\mu}\hat{E}_l - \mu E_l)\int_0^\infty \hat{\chi}_l\chi_l\,dr, \tag{16}$$

which can be rearranged to yield

$$2\overline{\mu}\Delta\mu\frac{\int (F_N(r)+F_C(r))\hat{\chi}_l\chi_l dr}{\int \hat{\chi}_l\chi_l dr}=\{\overline{\mu}(\Delta E_l)+\overline{E_l}(\Delta\mu)\}, \tag{17}$$

where $\Delta E_l=(\hat{E}_l-E_l)$, $\overline{E_l}=(\hat{E}_l+E_l)/2$, $\Delta\mu=(\hat{\mu}-\mu)$, and $\overline{\mu}=(\hat{\mu}+\mu)/2$. Similarly, for a different angular momentum $L>l$

$$2\overline{\mu}\Delta\mu\frac{\int (F_N(r)+F_C(r))\hat{\chi}_L\chi_L dr}{\int \hat{\chi}_L\chi_L dr}=\{\overline{\mu}(\Delta E_L)+\overline{E_L}(\Delta\mu)\} \tag{18}$$

Subtracting Eq. (17) from Eq. (18), and noting that for the states with many nodes $\chi_L=\chi_l$ and $\hat{\chi}_L=\hat{\chi}_l$ to a good approximation [9] (the main differences between the wave functions being confined to a small region close to the origin, $r=0$), results in

$$\frac{(\Delta E_L-\Delta E_l)}{\overline{E_L}-\overline{E_l}}=\frac{\Delta S_{Ll}}{\overline{S_{Ll}}}\sim-\frac{\Delta\mu}{\overline{\mu}}, \tag{19}$$

where S_{Ll} is the $L\rightarrow l$ energy spacing. Equation (19) is our principal result. We have derived it for bands B and $\hat{B}$ of a given nucleus described by core-cluster configurations having similar values of the reduced masses μ and $\hat{\mu}$, respectively, and for which functions F_N and F_C in Eqs. (12) and (13) have equal parameters and so remain the same. Thus, any changes in the band energies are driven by changes in μ and $\hat{\mu}$ only. We suggest that this remains approximately true for bands in neighboring even-even nuclei.

The quantity $\Delta S_{Ll}/\overline{S_{Ll}}$ defined in Eq. (19) would be the same for any pair of angular momentum values L and l as long as the band energies satisfy $\hat{E}_l=\hat{a}f(l)$ and $E_l=af(l)$, with f any function of l common to the two bands and $\hat{a}$ and a any two constants. In particular, this would apply with $f(l)=\hbar^2 l(l+1)$ to a pair of rotational bands of constant moments of inertia $\hat{I}$ and I, respectively. In practice, quantity $\Delta S_{Ll}/\overline{S_{Ll}}$ will depend to some extent on the chosen L and l, and for ND bands we choose $L=10$ and $l=0$ so as to include as large an energy difference as possible, while avoiding the effects of band crossing and mixing. At these low angular momentum values, there is usually a sizable energy gap to the next state with the same J^π value, suggesting that mixing cannot be very large. We thereby minimize the number of states which are dubious band members. This restriction to low L can be lifted if the bands being compared are believed to have a fixed structure and their members to be unambiguously assigned.

TABLE I. Normally deformed bands in rare-earth nuclei: data.

Nucleus	$\langle Z_2\rangle$	μ	$BE2\uparrow$ [13] $(e\,\mathrm{b})^2$
^{142}Ba	3.0	7.20	0.699±0.037
^{144}Ba	4.8	11.29	1.05±0.06
^{146}Ba	5.2	12.31	1.355±0.048
^{146}Ce	4.9	11.29	1.14±0.12
^{146}Nd	3.1	7.15	0.760±0.025
^{148}Ce	5.3	12.29	1.96±0.18
^{148}Nd	3.3	7.69	1.35±0.05
^{150}Nd	5.4	12.29	2.760±0.040
^{150}Sm	3.3	7.56	1.350±0.030
^{152}Nd	8.8	19.02	4.20±0.28
^{152}Sm	5.5	12.29	3.46±0.06
^{154}Sm	8.9	18.93	4.36±0.05

A. ND bands in light rare-earth and actinide nuclei

We next calculate values of $\Delta\mu/\overline{\mu}$ for pairs of ND ground state bands of the isotopes of Ba, Nd, Ce, and Sm in the light rare-earth region and of the isotopes of Ra, Th, U, and Pu in the actinide region. For these regions, previous calculations have shown that a cluster model description is appropriate [6,10,11], and in the present analysis we include all the above mentioned isotopes for which the $B(E2;0^+\rightarrow 2^+)$ value and the excitation energy of the lowest 10^+ state are known. In Tables I and II and in subsequent Tables, we order nuclei by ascending mass and for equal mass by ascending charge.

The ratio r of the cluster charge to the total charge is expected to satisfy $r\leqslant 1/6$ [12], i.e., $\langle Z_2\rangle\leqslant 12$ for the light

TABLE II. Normally deformed bands in actinide nuclei: data.

Nucleus	$\langle Z_2\rangle$	μ	$BE2\uparrow$ [13] $(e\,\mathrm{b})^2$
^{218}Ra	3.2	7.64	1.10±0.20
^{222}Ra	5.4	12.79	4.54±0.39
^{222}Th	5.1	11.87	3.01±0.32
^{224}Ra	5.9	14.01	3.99±0.15
^{226}Ra	7.4	17.40	5.15±0.14
^{226}Th	7.3	16.84	6.85±0.42
^{228}Th	8.6	19.71	7.06±0.24
^{230}Th	9.0	20.70	8.04±0.10
^{230}U	9.1	20.50	9.7±1.2
^{232}Th	9.4	21.70	9.28±0.10
^{232}U	9.3	21.08	10.0±1.0
^{234}Th	9.4	21.89	8.0±0.7
^{234}U	10.4	23.46	10.66±0.20
^{236}U	11.2	25.23	11.61±0.15
^{238}U	11.8	26.61	12.09±0.20
^{238}Pu	11.8	26.13	12.61±0.17
^{240}Pu	12.9	28.42	13.02±0.30
^{242}Pu	13.6	29.95	13.40±0.16
^{244}Pu	15.5	33.60	13.68±0.16

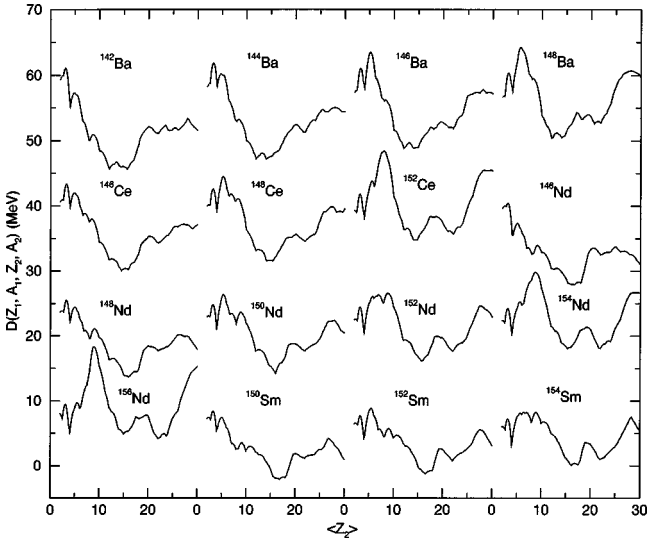

FIG. 1. Plots of $D(Z_1,A_1,Z_2,A_2)$ as functions of the cluster charge $\langle Z_2\rangle$ for the light rare-earth nuclei of Table I. The rows are displaced upwards by successive multiples of 15 MeV for more clarity.

rare-earths and $\langle Z_2\rangle \leqslant 16$ for the actinides. In Tables I and II, the value of the cluster charge $\langle Z_2\rangle$ for each nucleus has been chosen to correspond to the most prominent maximum in the appropriate region of the D plots of Figs. 1 and 2. These figures show sequences of the various isotopes so that the general evolution of the peak structure (and the implied cluster) can be tracked and seen to change fairly smoothly.

There is often a considerable small scale noisy structure in the D-plot curves, and when this is at its worst we can only expect ourselves to be able to specify the cluster charge to about ± 0.2 units. In fact, we follow the simple D-plot prescription for determining the cluster charge throughout, with the exception of ^{144}Ba and ^{146}Ce where we find that using the value of $\langle Z_2\rangle$ of a local maximum overlapping, and

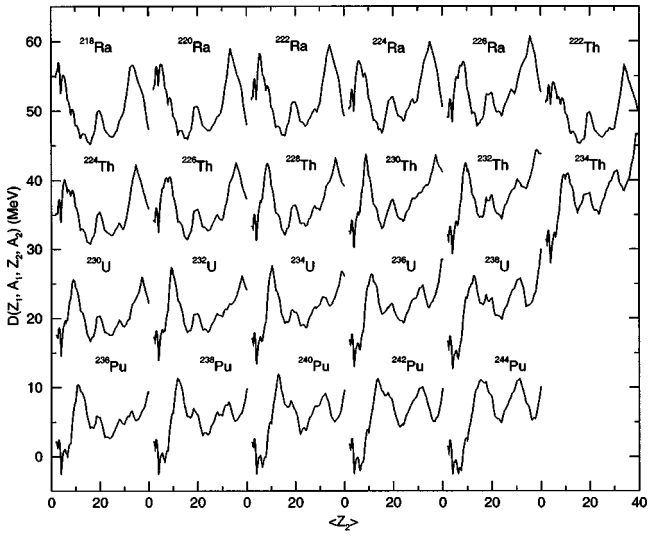

FIG. 2. Plots of $D(Z_1,A_1,Z_2,A_2)$ as functions of the cluster charge $\langle Z_2\rangle$ for the actinide nuclei of Table II. The rows are displaced upwards by successive multiples of 15 MeV for more clarity.

TABLE III. Normally deformed bands in rare-earth nuclei: results. a values of $-\Delta\mu/\overline{\mu}$ from D plots; b values of $-\Delta\mu/\overline{\mu}$ from $BE2\uparrow$'s; and c average of a and b.

Pair of nuclei	$-\Delta\mu/\overline{\mu}$			$\Delta S_{10,0}/\overline{S}_{10,0}$
	a	b	c	
^{142}Ba ^{144}Ba	0.442	0.200	0.321	0.355
^{144}Ba ^{146}Ba	0.086	0.127	0.107	−0.004
^{146}Ba ^{146}Ce	−0.086	−0.086	−0.086	−0.136
^{146}Ce ^{146}Nd	−0.449	−0.200	−0.325	−0.341
^{146}Nd ^{148}Ce	0.529	0.441	0.485	0.598
^{148}Ce ^{148}Nd	−0.461	−0.184	−0.323	−0.319
^{148}Nd ^{150}Nd	0.461	0.343	0.402	0.429
^{150}Nd ^{150}Sm	−0.477	−0.343	−0.410	−0.414
^{150}Sm ^{152}Nd	0.862	0.514	0.688	0.682
^{152}Nd ^{152}Sm	−0.430	−0.097	−0.264	−0.295
^{152}Sm ^{154}Sm	0.425	0.115	0.270	0.188

barely resolvable from the marginally most prominent one, leads to considerably improved results. Having chosen $\langle Z_2\rangle$ the no-dipole constraint of Eq. (4) gives the cluster mass A_2 corresponding to this charge and subtraction of this from the parent mass yields the core mass A_1. This allows an evaluation of $\mu = A_1A_2/(A_1+A_2)$ and hence $\Delta\mu/\overline{\mu}$ for any pair of nuclei. Of the nuclei listed in Tables I and II any one can be compared with any other, leading generally to a square matrix of comparisons. However, a lot of information in such a matrix would be redundant, and we avoid double counting in Tables III and IV by confining ourselves to successive

TABLE IV. Normally deformed bands in actinide nuclei: results. a, values of $-\Delta\mu/\overline{\mu}$ from D plots; b, values of $-\Delta\mu/\overline{\mu}$ from $BE2\uparrow$'s; and c, average of a and b.

Pair of nuclei	$-\Delta\mu/\overline{\mu}$			$\Delta S_{10,0}/\overline{S}_{10,0}$
	a	b	c	
^{218}Ra ^{222}Ra	0.504	0.610	0.557	0.503
^{222}Ra ^{222}Th	−0.075	−0.203	−0.139	−0.219
^{222}Th ^{224}Ra	0.165	0.140	0.153	0.310
^{224}Ra ^{226}Ra	0.216	0.127	0.172	0.107
^{226}Ra ^{226}Th	−0.033	0.142	0.055	−0.080
^{226}Th ^{228}Th	0.157	0.015	0.086	0.132
^{228}Th ^{230}Th	0.049	0.065	0.057	0.036
^{230}Th ^{230}U	−0.010	0.094	0.042	0.027
^{230}U ^{232}Th	0.057	−0.022	0.018	0.035
^{232}Th ^{232}U	−0.029	0.037	0.004	0.026
^{232}U ^{234}Th	0.038	−0.111	−0.037	−0.045
^{234}Th ^{234}U	0.069	0.144	0.107	0.129
^{234}U ^{236}U	0.073	0.043	0.058	−0.054
^{236}U ^{238}U	0.053	0.020	0.037	0.008
^{238}U ^{238}Pu	−0.018	0.021	0.002	0.004
^{238}Pu ^{240}Pu	0.084	0.016	0.050	0.033
^{240}Pu ^{242}Pu	0.052	0.014	0.033	−0.041
^{242}Pu ^{244}Pu	0.115	0.010	0.063	−0.025

pairs of nuclei from Tables I and II.

An independent estimate of $\Delta\mu/\bar{\mu}$ can be obtained from the measured values of the electric quadrupole transition strengths $B(E2;0^+\rightarrow 2^+)=BE2\uparrow$ shown in Tables I and II. Taking into account the dipole condition of Eq. (4), the cluster model expression for this quantity is given by

$$BE2\uparrow=\frac{5}{4\pi}\left(\frac{Z_1Z_2}{Z_T}\right)^2\left(\int \chi_0(r)r^2\chi_2(r)dr\right)^2 \sim \frac{5}{4\pi}\left(\frac{Z_1Z_2}{Z_T}\right)^2\left(\int \chi_0^2(r)r^2dr\right)^2\sim\frac{5}{4\pi}\mu^2\frac{Z_T^2}{A_T^2}(r_0^2A_T^{2/3})^2, \tag{20}$$

where we have replaced $\chi_2(r)$ by $\chi_0(r)$ [see discussion after Eq. (18)], and approximated $\langle r^2\rangle$ by $r_0^2A_T^{2/3}$ (with r_0 some constant). Since the fractional changes in Z_T and A_T are small for the neighboring heavy nuclei considered here, we immediately find that our cluster model gives rise to the simple, parameter-free relation

$$\frac{\Delta\mu}{\bar{\mu}}=\frac{1}{2}\frac{\Delta(BE2\uparrow)}{BE2\uparrow}. \tag{21}$$

Our results for $-\Delta\mu/\bar{\mu}$ obtained by the two independent methods above are shown in Table III for the light rare earths, and in Table IV for the actinides, and are seen generally to support each other in these mass regions, where the *D*-plot maxima are reasonably clear-cut. This is not the case for the heavier rare-Earths, where the *D*-plot maxima are broader and less well defined. Here, the technique based on the $BE2\uparrow$ values and Eqs. (20) and (21) is more definite and will allow us to extend our cluster model comparisons to this region in future. To reduce uncertainties as far as possible, we use the average of the estimates of the cluster charges generated by these two methods. These are sufficiently close to one another such that no significant errors are made by taking directly, for convenience, the average of the $\Delta\mu/\bar{\mu}$ ratios.

In the present study, the average values of $-\Delta\mu/\bar{\mu}$ from the two methods quite closely track the quantities $\Delta S/\bar{S}=\Delta S_{10,0}/\bar{S}_{10,0}$ (which measure the similarity of a pair of bands), and in Fig. 3 we show a plot of these quantities together with the error in $-\Delta\mu/\bar{\mu}$ calculated from the difference of the two independent estimates of the latter. Also shown is the theoretical line $-\Delta\mu/\bar{\mu}=\Delta S/\bar{S}$, which effectively fits the results and strongly supports the conjecture that a greater degree of similarity of the two bands is to be associated with a smaller value of $|\Delta\mu/\bar{\mu}|$.

It should be pointed out that the slope of -1 in this plot is *twice* that expected from the energy dependence of the usually employed relation between $B(E2)$ strengths and 2^+ excitation energies [13] based on the original work of Grodzins [14,15]. It is probable that this difference is largely due to the contribution of the pairing energy to the 0^+-2^+ energy difference. It is important to reduce this influence by choosing as large an L value as possible for the other comparison state in the two bands (or even to avoid using the ground state at all).

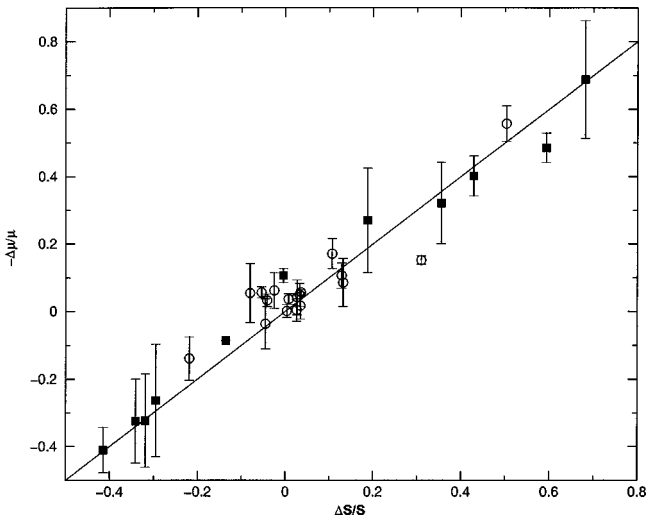

FIG. 3. $-\Delta\mu/\bar{\mu}$ against $\Delta S/\bar{S}$ for the actinide (open circles) and rare-Earth (filled squares) nuclei under consideration. The error bars indicate the difference in $\Delta\mu/\bar{\mu}$ from the two independent methods discussed in the text. For comparison, a line of unit gradient has been drawn through the origin.

To summarize, the strength of the correlation between two variables x and y may be usefully measured by the correlation coefficient r defined as

$$r=\frac{n\sum xy-\left(\sum x\right)\left(\sum y\right)}{\sqrt{\left[n\sum x^2-\left(\sum x\right)^2\right]\left[n\sum y^2-\left(\sum y\right)^2\right]}}, \tag{22}$$

where there are n data points available. We use this expression to give a numerical measure of the correlation between $\langle\Delta S/\bar{S}\rangle$ and $-\Delta\mu/\bar{\mu}$ and find that $r=0.973$ for the 29 entries of the last two columns of Tables III and IV, indicating a very significant degree of correlation between these quantities.

Another work which also results in a simple, reasonably successful, model-based indicator of similarity is that of Refs. [16,17], which uses the quantity $N_pN_n/(N_p+N_n)$, with N_p and N_n the number of protons and neutrons, respectively, outside a closed shell. We believe that the success of both the other analysis and our own suggests that parallels can be drawn between the N_pN_n scheme and the cluster model [18]. In the present work, we deduce from the linear fit of Fig. 3 that identical bands are simply a sporadically occurring special case of similarity, and that ''their appearance is not an isolated exception to the normal behavior of nuclei [17].''

B. SD bands for $A\sim$ 150 and 190

In this section, we wish to compare similar superdeformed bands using the same criteria as previously applied to

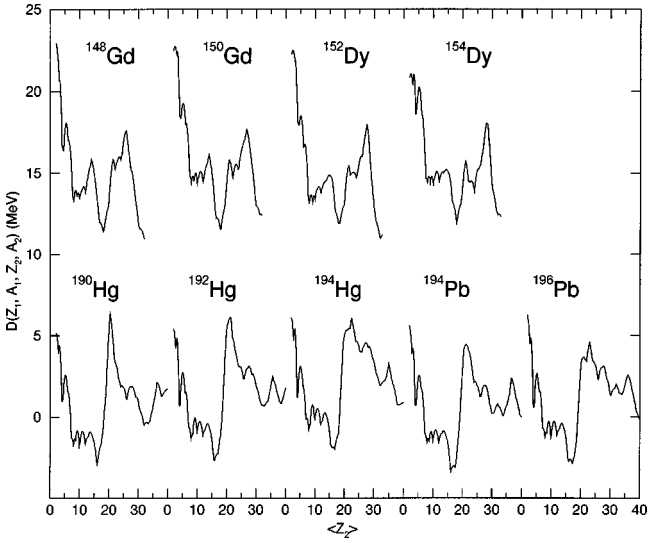

FIG. 4. Plots of $D(Z_1,A_1,Z_2,A_2)$ as functions of the cluster charge $\langle Z_2\rangle$ for the rare-earth and actinide nuclei of Tables III–V. The curves for the rare-earth nuclei are shifted upwards by 15 MeV for more clarity.

normal deformed ground state bands. We pick a selection of nuclei in the mass 150 and mass 190 ranges whose transition quadrupole moments we have previously been able to describe in terms of a cluster model [12], making it likely that a cluster model is appropriate for their description. Although SD bands include near-identical cases, and so yield very similar comparison ratios, the very smallness of the differences between these ratios makes their calculation highly sensitive to the quality of input information. We do not expect to reproduce these small quantities exactly, but only to demonstrate that the small variations in the large cluster-core reduced masses associated with them will generate more closely similar bands than we had in the ND cases.

Despite being potentially the best testing grounds for our ideas, the present experimental data on SD bands are not ideally suited to our task and present considerable difficulties. One such practical difficulty is that there are often several SD bands in a given nucleus on which we could base our comparisons. Since the implied moments of inertia of such bands are closely similar, we have arbitrarily chosen the bands labeled as "band (1)" [3], except for ^{148}Gd where band (1) refers to an odd-J band. A further difficulty is that we rarely know with certainty the spins of the states involved. We adopt the values of Ref. [3] and evaluate $\Delta S_{Ll}/\overline{S_{Ll}}$ by using extremal L and ℓ-values common to the SD bands in all the neighboring nuclei (we believe the underlying structure to be fixed in these bands). This leads us to limit the spin range from 34 to 62 for the rare-earth nuclei and from 14 to 38 for the heavy metals Hg/Pb.

Figure 4 shows the D plots for the nuclei in question, and clearly shows maxima around $\langle Z_2\rangle \sim 26$ for all the rare-earths and around $\langle Z_2\rangle \sim 22$ for all the heavy metal Hg/Pb isotopes of interest. These peaks often have a small amount of substructure which limits the accuracy of the deduced cluster charge somewhat (to about ± 0.2). Table V summarizes the cluster charges and associated reduced masses

TABLE V. Superdeformed bands in rare-earth and heavy metal Hg/Pb nuclei: data.

Nucleus	$\langle Z_2\rangle$	μ	Band label [3]	L range available/ used	Q_t [3] (e b)
^{148}Gd	25.9	35.655	^{148}Gd(2)	34–64/34–62	14.8 ± 0.3
^{150}Gd	26.8	36.510	^{150}Gd(1)	34–64/34–62	$17.0^{+0.5}_{-0.4}$
^{152}Dy	27.6	36.982	^{152}Dy(1)	26–66/34–62	17.5 ± 0.2
^{154}Dy	28.1	37.651	^{154}Dy	30–64/34–62	$15.9^{+3.1}_{-2.1}$
^{190}Hg	20.4	36.095	^{190}Hg(1)	14–42/14–38	$17.7^{+1.0}_{-1.2}$
^{192}Hg	21.3	37.509	^{192}Hg(1)	10–48/14–38	20.2 ± 1.2
^{194}Hg	22.5	39.217	^{194}Hg(1)	10–50/14–38	17.7 ± 0.4
^{194}Pb	21.3	37.303	^{194}Pb(1)	6–38/14–38	$20.1^{+0.3}_{-0.5}$
^{196}Pb	21.0	37.340	^{196}Pb(1)	8–38/14–38	$19.5^{+0.4}_{-0.3}$

adopted for the calculations as well as indicating the experimental data sources and spin ranges for the associated experimental comparison. In choosing cluster charges $\langle Z_2\rangle$ for SD bands, we follow a similar procedure to the one adopted in Sec. IV A for ND bands. For each nucleus, we thus associate the optimal $\langle Z_2\rangle$ with the most prominent maximum of the relevant D plot of Fig. 4, in the region where the cluster to total charge ratio $r \geqslant 1/6$ [12]. We adopt this simple prescription throughout, except for ^{196}Pb, where the situation is ambiguous and the choice of $\langle Z_2\rangle = 21.0$ (corresponding to the local maximum adjacent to the most prominent one at $\langle Z_2\rangle = 23.0$) much improves the results involving this nucleus.

As for the ND bands in Sec. IV A, a further estimate of $\Delta\mu/\overline{\mu}$ can be made using the measured values of the transition quadrupole moment Q_t shown in Table V. A similar derivation to that leading to Eq. (20) results in

$$Q_t \approx 2\mu \frac{Z_T}{A_T}(r_0^2 A_T^{2/3}) \tag{23}$$

so that

$$\frac{\Delta\mu}{\overline{\mu}} = \frac{\Delta Q_t}{Q_t}. \tag{24}$$

Possible improvements in the precision of these measurements would enhance our comparisons considerably.

Table VI summarizes our results, and shows that the value of $-\Delta\mu/\overline{\mu}$ continues to give a reasonable semiquantitative account of the data even in the worst cases. We also note that $\Delta\mu/\overline{\mu}$ from the D plots agree rather better with $\Delta S/\overline{S}$ than do the corresponding values from the Q_t's, and that this is a likely consequence of the experimental uncertainties in the latter. At some cost to clarity, the SD results of Table VI could be included in Fig. 3. These would then group close to the origin underlining the conclusion that greater degrees of similarity between the two bands, i.e., smaller values of $|\Delta S/\overline{S}|$, are associated with smaller values of $|\Delta\mu/\overline{\mu}|$.

TABLE VI. Superdeformed bands in rare-earth and heavy metal Hg/Pb nuclei: results. For ranges of ℓ, L used see Table V. *a*, values of $-\Delta\mu/\overline{\mu}$ from D plots; *b*, values of $-\Delta\mu/\overline{\mu}$ from Q_t's; and *c*, average of *a* and *b*.

Pair of nuclei	$-\Delta\mu/\overline{\mu}$			$\Delta S_{L,\ell}/\overline{S}_{L,\ell}$
	a	*b*	*c*	
^{148}Gd(2) ^{150}Gd(1)	0.024	0.138	0.081	0.025
^{150}Gd(1) ^{152}Dy(1)	0.013	0.029	0.021	−0.004
^{152}Dy(1) ^{154}Dy(1)	0.018	−0.095	−0.039	−0.009
^{190}Hg(1) ^{192}Hg(1)	0.038	0.132	0.085	0.045
^{192}Hg(1) ^{194}Hg(1)	0.045	−0.132	−0.044	0.010
^{194}Hg(1) ^{194}Pb(1)	−0.050	0.126	0.038	−0.012
^{194}Pb(1) ^{196}Pb(1)	0.001	−0.030	−0.015	−0.023

The results of Tables III, IV, and VI are consistent with the general finding that closely similar bands in even-even nuclei have been observed for SD rather than ND bands. This is explained in the cluster model by noting that prominent maxima in the D plots are generally associated with magic cores (see, e.g., Refs. [4,6] and Figs. 1, 2, and 4). For adjacent heavy even-even nuclei (i.e., differing by two mass units), an *unchanging* core implies $A\rightarrow A_2+(A-A_2)$ and $(A+2)\rightarrow(A_2+2)+(A-A_2)$ corresponding to $-\Delta\mu/\overline{\mu}\sim 2/A_2$, where A_2 is the cluster mass. Since the A_2's associated with ND and SD structures are typically $\sim$(10–20) and $\sim$(50–100) mass units, respectively, it is clear that in such a situation closely similar bands will be associated with superdeformation.

V. PREDICTIONS FOR ^{212}Pb AND ^{212}Po

We turn next to an application of the cluster model to ^{212}Pb and ^{212}Po, partly to give a model interpretation of their ground state ND bands, but also to predict the existence and the properties of very similar SD bands in these nuclei. In Fig. 5, we show both unsmoothed and smoothed versions of the D plots for these nuclei [6]. We elect here to use the better defined maxima of the latter, noting that in any event our conclusions are little affected by this choice. The strong maxima in our D plots of Fig. 5 make the choice of likely core-cluster combinations for ^{212}Pb and ^{212}Po quite unambiguous. For the ND bands, a predominantly α-cluster structure is predicted for both nuclei, and indeed the excitation energies of members of their ground state bands are similar at (0.805,0.727), (1.117,1.132), (1.277,1.355), and (1.335, 1.476) MeV for the $J^\pi=2^+,4^+,6^+$, and 8^+ states of (^{212}Pb, ^{212}Po), respectively [19]. Previous applications of the cluster model to ^{212}Po gave an overall good picture of the α- and γ-decay properties of the ground state band [20,21].

As no further information on the ND ground state bands of ^{212} Pb and ^{212}Po is available (other than the $J^\pi=2^+$ to 8^+ excitation energies of the ground state band of ^{212}Pb), we proceed to examine the possible SD bands in these nuclei, with which we associate the maxima in the D plots of Fig. 5 at $\langle Z_2\rangle=30.9$ and $\langle Z_2\rangle=31.8$ for ^{212}Pb and ^{212}Po, respectively. Application of the dipole rule of Eq. (4) yields $\langle A_2\rangle$

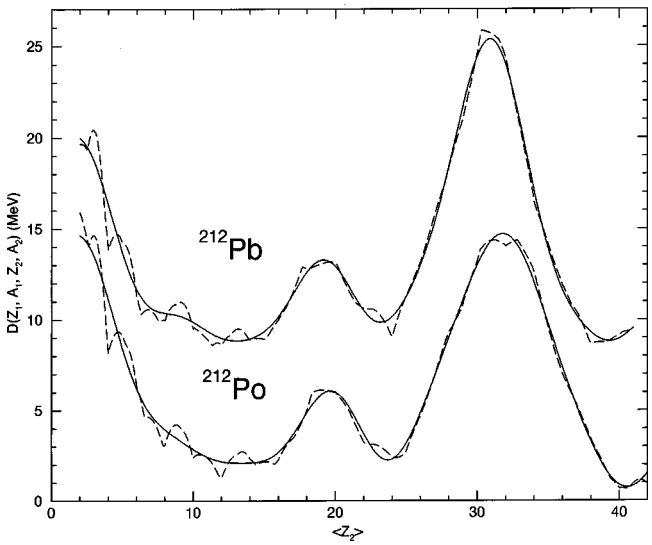

FIG. 5. Plots of $D(Z_1,A_1,Z_2,A_2)$ as functions of the cluster charge $\langle Z_2\rangle$ for ^{212}Pb and ^{212}Po. The dashed curve gives the results of Eq. (1), and the solid curve gives a Fourier based smoothing of them. The curves for ^{212}Pb are shifted upwards by 5 MeV for more clarity.

$=79.9$ and $\langle A_2\rangle=80.3$, and hence $|\Delta\mu/\overline{\mu}|=2\times10^{-3}$, implying that such bands should be very similar indeed. We thus perform model calculations for ^{212}Po only. For simplicity we use a single even-even cluster approximation with $Z_2=32, A_2=80$, and confine ourselves to transition energies within the SD band, which are very insensitive to the unknown $J^\pi=0^+$ bandhead energy, arbitrarily set at 5.0 MeV. For the Q value of the head of the band described as ^{132}Te $+^{80}$Ge, we thus obtain $Q=149.208$ MeV. The core-cluster potential is defined by Eqs. (8), (9), and (11), with parameter values given by Eq. (10). The remaining parameter R is obtained by fitting the Q value above, using an estimate for the global quantum number $G=0.88A_1A_2/(A_1+A_2)^{2/3}$ [4]. The calculations were performed using the Bohr-Sommerfeld semiclassical approximation

$$\int_{r_1}^{r_2}\sqrt{\frac{2\mu}{\hbar^2}\left(Q_L-V_N(r)-V_C(r)-\frac{\hbar^2(L+1/2)^2}{2\mu r^2}\right)}dr = (G-L+1)\frac{\pi}{2} \tag{25}$$

(where r_1 and r_2 are the classical turning points), which yields accurate values for the energy differences $(\Delta Q)_{Ll}$

TABLE VII. Energy differences $(\Delta Q)_{Ll}=Q_L-Q_l$ and nominal excitation energies for a predicted SD band of ^{212}Po. A nearly identical band in ^{212}Pb should shadow these results very closely.

L	l	$(\Delta Q)_{Ll}$ (MeV)	E_L^* (MeV)
10^+	0^+	0.454	5.454
20^+	10^+	1.172	6.626
30^+	20^+	1.762	8.388

$=Q_L-Q_l$ of members of the band of angular momentum L and l. This gives $R=6.288$ fm and the results shown in Table VII. We find that the transition energies are fairly sensitive to the assumed value for G and increase by $\sim 10\%$ for a 4% decrease in G. Finally, given the core-cluster decomposition for the band, it is easy to make a robust estimate [12] of its transition quadrupole moment as $Q_t=23.9\ e$ b.

VI. CONCLUSIONS

We have shown that, in a cluster model, the fractional change in the reduced mass of the core and the cluster is the principal factor in determining the fractional change in the transition energies of similar bands in neighboring even-even nuclei. We emphasize that $|\Delta\mu/\overline{\mu}|$ agrees well with $|\Delta S/\overline{S}|$ in almost all cases. Hence, large $|\Delta\mu/\overline{\mu}|$ implies dissimilar bands, while very small $|\Delta\mu/\overline{\mu}|$ implies closely similar bands. It then follows straightforwardly from a description of nuclei as binary cluster systems that closely similar bands will be associated with SD rather than ND bands, because of their larger values of cluster mass, in agreement with observations. A firm prediction of the model is that nearly identical SD bands should occur in the $A\sim 210$ region specifically for ^{212}Pb and ^{212}Po.

ACKNOWLEDGMENTS

S.M.P. would like to thank the S. A. Foundation for Research, the University of Cape Town, and the EPSRC for financial support.

[1] T. Byrski *et al.*, Phys. Rev. Lett. **64**, 1650 (1990).
[2] C. Baktash, B. Haas, and W. Nazarewicz, Annu. Rev. Nucl. Part. Sci. **45**, 485 (1995).
[3] Xiao-Ling Han and Cheng-Li Wu, At. Data Nucl. Data Tables **73**, 43 (1999).
[4] B. Buck, A.C. Merchant, M.J. Horner, and S.M. Perez, Nucl. Phys. **A673**, 157 (2000).
[5] B. Buck, A.C. Merchant, and S.M. Perez, Few-Body Syst. **29**, 53 (2000).
[6] B. Buck, A.C. Merchant, M.J. Horner, and S.M. Perez, Phys. Rev. C **61**, 024314 (2000).
[7] W. S. C. Williams, in *Nuclear and Particle Physics* (Clarendon, Oxford, 1991), p. 60.
[8] B. Buck, A.C. Merchant, and S.M. Perez, Nucl. Phys. **A614**, 129 (1997).
[9] B. Buck, A.C. Merchant, and S.M. Perez, Phys. Rev. C **57**, R2095 (1998).
[10] B. Buck, A.C. Merchant, and S.M. Perez, Nucl. Phys. **A652**, 211 (1999).
[11] B. Buck, A.C. Merchant, and S.M. Perez, Nucl. Phys. **A657**, 267 (1999).
[12] B. Buck, A.C. Merchant, and S.M. Perez, Phys. Rev. C **63**, 014312 (2000).
[13] S. Raman, C.W. Nestor, Jr., and P. Tikkanen, At. Data Nucl. Data Tables **78**, 1 (2001).
[14] L. Grodzins, Phys. Lett. **2**, 88 (1962).
[15] B. Buck, A.C. Merchant, V.A. McBride, and S.M. Perez, Phys. Rev. C **66**, 067303 (2002).
[16] R.F. Casten, N.V. Zamfir, P. von Brentano, and W.-T. Chou, Phys. Rev. C **45**, R1413 (1992).
[17] J.-Y. Zhang, R.F. Casten, W.-T. Chou, D.S. Brenner, N.V. Zamfir, and P. von Brentano, Phys. Rev. Lett. **69**, 1160 (1992).
[18] B. Buck, A. C. Merchant, and S. M. Perez (unpublished).
[19] A. Artna-Cohen, Nucl. Data Sheets **66**, 171 (1992).
[20] B. Buck, A.C. Merchant, and S.M. Perez, Phys. Rev. Lett. **72**, 1326 (1994).
[21] B. Buck, J.C. Johnston, A.C. Merchant, and S.M. Perez, Phys. Rev. C **53**, 2841 (1996).